IEEE Access
Multidisciplinary | Rapid Review | Open Access Journal

Received October 8, 2019, accepted October 24, 2019, date of publication November 4, 2019, date of current version November 14, 2019.

Digital Object Identifier 10.1109/ACCESS.2019.2950991

The Apparent Density Mapping Approach in Spherical Coordinates and the Crustal Density Distribution of Chinese Mainland

AOWEI HAO, LIANGHUI GUO, AND XIANG WANG
School of Geophysics and Information Technology, China University of Geosciences, Beijing 100083, China

Corresponding author: Lianghui Guo (guo_lianghui@163.com)

This work was supported in part by the National Natural Science Foundation of China under Grant 41774098 and Grant 41974101, and in part by the Fundamental Research Funds for Central Universities.

ABSTRACT Apparent density mapping is a technique to obtain lateral density distribution of subsurface layer by inverting gravity anomaly. In general, the subsurface layer can be divided into vertical, juxtaposed prisms in Cartesian coordinates. However, for continental and global scales, the curvature of the earth should be taken into account, and the subsurface layer should be divided into Tesseroids in spherical coordinates instead of rectangular prisms. In this paper, we present a modified Gauss-Legendre algorithm to forward the gravity anomaly generated by an arbitrary Tesseroid, and the precision can be improved vastly when the observation points in the near surface of the Tesseroid. The shell tests show that the relative maximum error can be controlled in 0.0009343% when the Gauss-Legendre nodes are set as (4, 4) in the longitude and latitude directions and the subdivision parameter W is set as 1.5. Then, an apparent density mapping approach is presented in spherical coordinates to minimize the difference between the observed gravity anomalies and calculated gravity anomalies. The synthetic model verified the feasibility and precision of our approach. In real application, we have obtained the crustal apparent density distribution of Chinese mainland with $0.25° \times 0.25°$ in longitude and latitude directions. The crustal apparent distribution of Chinese mainland is generally low in the western region and high in eastern region varying from 2.45-2.81 g/cm^3 and closely related to lithologic units and geological boundaries.

INDEX TERMS Gravity inversion, apparent density mapping, spherical coordinates, Chinese mainland.

I. INTRODUCTION

The gravity method is a popular tool for geologic mapping and tectonic studies for decades [1]–[6]. Density, as an essential parameter of gravity inversion, is closely related to types of rocks and tectonic evolution. Apparent density mapping [2]–[6] is a technique to estimate the spatial distribution of the density of the subsurface layer from the observed gravity data. Unlike the true density measured directly on a limited number of rock specimens, apparent density is an average of the rock density of a certain depth below each observed station. This technique is beneficial to identifying lithologic units and delineating geological boundaries.

In Cartesian coordinates, the technique of apparent density mapping usually divides the subsurface layer, whose top and bottom surfaces are assumed to be horizontal or variable depth, into a grid of vertical, juxtaposed prisms in both horizontal directions. Then, the density of each prism can be derived from gravity anomalies by using the mapping algorithm. Many frequency-domain algorithms of apparent density mapping have been utilized for decades, mainly including frequency-domain deconvolution [1], [2], terracing operator [7], Walsh transform [3], Wiener filter and Green's equivalent layer principles [4], entropic regularization [5], and wavenumber-domain iterative approach [6]. Although the frequency-domain algorithms are fast and convenient, they require that the observation surface is flat without topographical variation, which is not generally the case in real word. Meanwhile, the curvature of the earth should be taken into account for continental and global scales [8]–[10], and it is obviously unavailable to use the mapping algorithms above in Cartesian coordinates. In this paper, the principle of

The associate editor coordinating the review of this manuscript and approving it for publication was Jenny Mahoney.

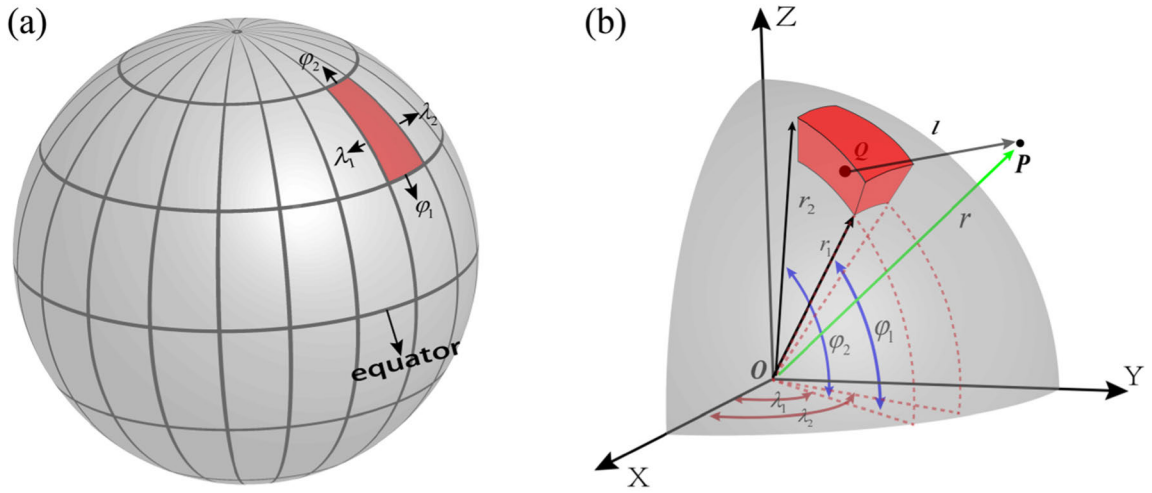

FIGURE 1. (a) The geometry of a Tesseroid in geographical boundary lines with longitudes (λ_1, λ_2) and latitudes (φ_1, φ_2), and (b) the 3-D display of a Tesseroid in spherical coordinates.

apparent density mapping in spherical coordinates is similar to that in Cartesian coordinates. The Tesseroid (Figure 1), which is an elementary unit in the spherical coordinates [10] is used instead of rectangular prism.

In general, there has no analytical solution to calculate gravity effects of a Tesseroid and the integral formula can only be solved numerically. The forward algorithm of the Tesseroid has been extensively discussed in recent decades [8], [9], [11]–[20]. The most widely used methods to calculate the gravity effect of a Tesseroid are Taylor-series expansion and Gauss-Legendre quadrature(GLQ).

The accuracy of Taylor series expansion is related to the order of expansion, and the more order means higher precision [14]–[16]. However, the formula of Taylor series expansion is cumbersome and complex. The GLQ is the approximate volume integral by a weighted sum of the effect of point massed and the precision can be determined by the total point numbers of the three different integral intervals [18]–[20]. Meanwhile, lots of remarkable methods [8], [9], [18], [21] have been applied to improve the precision of gravity effect generated by a Tesseroid. Ku proposed an empirical criterion that the distance between point masses should not be greater than the distance to the computer point to improve the precision of the GLQ integration [21]. Based on the criterion of Ku, Li *et al.* subdivided the Tesseroid into smaller ones by recursive function instead of increasing the number of point masses of per Tesseroid [18]. Uieda et al. proposed a modified adaptive algorithm to guarantee the precision the GLQ integration. A stack-based algorithm is used to instead of recursion, and the precision of the GLQ integration and computation time can be controlled by a scalar value [9]. In addition, Gravity inversion methods in spherical coordinates have been applied to satellite gravity data on moon for recent years [22]–[24], which are unsuitable for the surface gravity data due to poor numerical precision when the observation points in the near surface of the Tesseroid. Hence, the new algorithm is still needed to improve the precision when the computation points in the near surface of the Tesseroid.

In this paper, we present an apparent density mapping approach for the surface gravity data of the earth in spherical coordinates, and the top and bottom of subsurface layer can be constant or variable. First, we improved a modified algorithm called 2-GLQ to forward the gravitational acceleration generated by a Tesseriod. Secondly, we present a modified adaptive subdivision algorithm to guarantee the precision of 2-GLQ when the computation points in the near surface of the Tesseroid. Thirdly, a forward algorithm is available to calculate the gravity anomalies of observed points generated by a subsurface density layer, which can be divided into a series of Tesseriods. Then, we propose an inversion approach to calculate the density distribution of the subsurface layer. Finally, the test of the synthetic data verified the feasibility and precision of our approach. The results of crustal apparent density distribution of Chinese mainland are closely related to regional lithologic units and geological boundaries.

II. METHDOLOGY

A. FORWARD CALCULATION OF GRAVITY ANOMALY CAUSED BY A TESSEROID

1) THE MODIFIED GLQ ALGORITHM

The Tesseroid first introduced by Anderson can be defined as a basic spherical unit with six parameters: the geographical boundary lines with longitudes (λ_1, λ_2) and latitudes (φ_1, φ_2), and constant spherical radii (r_2, r_1) (see Figure1) [10].

Assume that the Tesseroid has a homogeneous mass-density, the gravitational potential V of point P generated by the Tesseroid can be expressed as:

$$V(r, \varphi, \lambda) = G\rho \int_{\lambda_1}^{\lambda_2} \int_{\varphi_1}^{\varphi_2} \int_{r_1}^{r_2} \frac{r'^2 \cos\varphi'}{l} dr' d\varphi' d\lambda', \quad (1)$$

$$l = \sqrt{r'^2 + r^2 - 2rr'\cos\psi}, \tag{2}$$

$$\cos\psi = \sin\varphi'\sin\varphi + \cos\varphi\cos\varphi'\cos\left(\lambda - \lambda'\right). \tag{3}$$

where G is the Newtonian gravitational constant, r, φ, λ and r', φ', λ' are the computation point P and integration point Q in spherical coordinates. l is the Euclidean distance between point Q and P, and ψ is the angle between the position vectors of points Q and P as spherical distance.

Then, the gravitational acceleration, by the reduction of the gravitational potential, results from [14], then we can get

$$\begin{aligned} g(r, \varphi, \lambda) &= -\frac{\partial V(r, \lambda, \varphi)}{\partial r} \\ &= G\rho \int_{\lambda_1}^{\lambda_2}\int_{\varphi_1}^{\varphi_2}\int_{r_1}^{r_2} \frac{r'^2 (r - r'\cos\psi)\cos\varphi'}{l^3} dr' d\varphi' d\lambda', \end{aligned} \tag{4}$$

The equation (4) can be simplified to double integral by reduce the r' [14], [25]. Then, we can get

$$\begin{aligned} g(r, \varphi, \lambda) = \frac{G\rho}{r}\int_{\lambda_1}^{\lambda_2}\int_{\varphi_1}^{\varphi_2} \cos\varphi' \Big[\frac{r'^3}{l} - l\left(r' + 3r\cos\psi\right) \\ - r^2(3\cos^2\psi - 1) \\ \times \ln\left(l + r' - r\cos\psi\right)\Big]\Big|_{r'=r_1}^{r'=r_2} d\varphi' d\lambda'. \end{aligned} \tag{5}$$

The equation (5) can be evaluated numerically and expressed as the generalized double integral obviously.

$$\int_{\varphi'=\varphi_1}^{\varphi_2}\int_{\lambda'=\lambda_1}^{\lambda_2} f\left(r, \lambda, \varphi, \lambda', \varphi', r_1, r_2\right) d\varphi' d\lambda', \tag{6}$$

Based on the theories of [15], [19], [26], [27],The least-squares numerical solution of Eq. (6) can be expressed by Gauss-Legendre quadrature decomposition

$$\begin{aligned} &\int_{\varphi'=\varphi_1}^{\varphi_2}\int_{\lambda'=\lambda_1}^{\lambda_2} f\left(r, \lambda, \varphi, \lambda', \varphi', r_1, r_2\right) d\varphi' d\lambda' \\ &\quad = A\sum_{nj=1}^{J}\sum_{ni=1}^{I} \omega_{ni}\omega_{nj} f\left(r, \lambda, \varphi, \hat{\lambda}'_{ni}, \hat{\varphi}'_{nj}, r_1, r_2\right), \end{aligned} \tag{7}$$

$$\hat{\lambda}'_{ni} = \frac{\lambda_{ni}(\lambda_2 - \lambda_1) + (\lambda_2 + \lambda_1)}{2},$$

$$\hat{\varphi}'_{nj} = \frac{\varphi_{nj}(\varphi_2 - \varphi_1) + (\varphi_2 + \varphi_1)}{2}. \tag{8}$$

where $A = (\lambda_2 - \lambda_1)(\varphi_2 - \varphi_1)/4$, I and J are the numbers of Gaussian-Legendre nodes in longitude and latitude directions, respectively. ω_{ni}, ω_{nj} are the n-th Gauss-Legendre coefficients. λ_{ni}, φ_{nj} are the n-th Gaussian-Legendre node in interval $[-1, 1]$, and $\hat{\lambda}'_{ni}$, $\hat{\varphi}'_{nj}$ are the real Gaussian-Legendre node coordinates within the Tesseroid. The function f can be calculated with $I \times J$ optimal points. The precision of the solution can be affected by many parameters, such as the numbers of the nodes, the size of the Tesseroid and the distance between the Tesseroid and the observation point [9], [18]–[20]. Our modified GLQ algorithm (2-GLQ) is described by generalized double integral. Assume that I, J, K are the Gauss-Legendre nodes in longitude, latitude and radius directions, respectively. The total point number for GLQ is I × J × K. As for the 2-GLQ, there is an integral analytic solution to the direction of the radius, which means the total weighted point number of 2-GLQ is I × J. The number of weighted point has been reduced by K times and the computation time can be improved greatly.

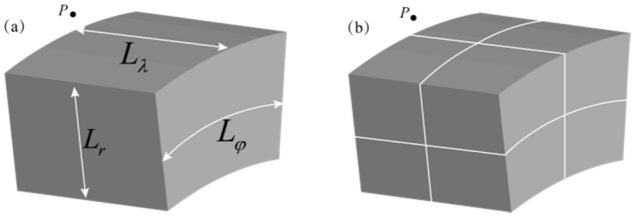

FIGURE 2. (a) Adaptive modified criteria of the Tesseroid for the computation point P, and L_λ, L_φ, L_r are the "side lengths" of longitude, latitude and radius, respectively. (b) The subdivision of the Tesseroid (a) into 8 smaller Tesseroid units in spherical coordinates when W is unavailable for (15).

2) ADAPTIVE CRITERIA OF A TESSEROID

To improve the precision when the computation points in the near surface of the Tesseroid, we implement a modified adaptive recursive algorithm, which has combined the advantages of recursive function [18] and adaptive stack based algorithm [9]. Assume that the range of the Tesseroid to be calculated is $[\lambda_k, \lambda_{k+1}]$, $[\varphi_k, \varphi_{k+1}]$, $[r_k, r_{k+1}]$ in longitude, latitude and radius directions, respectively (Figure 2a).Instead of the smallest distance, the distance between the geometric center of the Tesseroid $(r_m, \lambda_m, \varphi_m)$ and the computation point $P(r, \lambda, \varphi)$ (Figure 2a) can be followed as:

$$d = \sqrt{r^2 + r_m^2 - 2rr_m\cos\psi_m}, \tag{9}$$

$$\cos\psi_m = \sin\varphi\sin\varphi_m + \cos\varphi\cos\varphi_m\cos\left(\lambda - \lambda_m\right). \tag{10}$$

Meanwhile, the "side lengths" of three different dimensions [18] in spherical coordinates can be defined as:

$$L_\lambda = r_{k+1}\arccos\left(\sin^2\varphi_m + \cos^2\varphi_m\cos\left(\lambda_{k+1} - \lambda_k\right)\right), \tag{11}$$

$$L_\varphi = r_{k+1}\arccos\left(\sin\varphi_{k+1}\sin\varphi_k + \cos\varphi_{k+1}\cos\varphi_k\right), \tag{12}$$

$$L_r = r_{k+1} - r_k, \tag{13}$$

$$L_{max} = \max\left(L_r, L_\lambda, L_\varphi\right). \tag{14}$$

where, L_λ is arc-distance along the middle latitude of the top surface of the Tesseroid, and L_φ is arc-distance along the longitude of the top surface of the Tesseroid. L_{max} is the largest "side lengths" of the L_r, L_λ, L_φ.

The following formula is used to decide whether a Tesseroid should be subdivided. That is

$$W \le \frac{d}{L_{max}}. \tag{15}$$

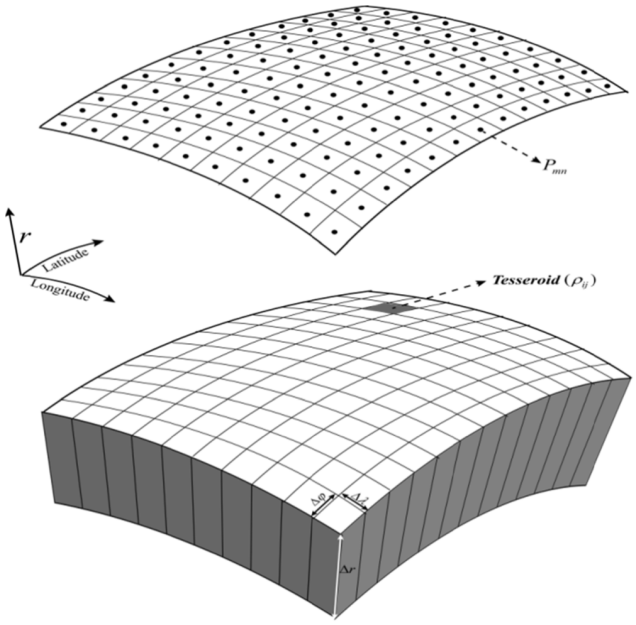

FIGURE 3. A subsurface density layer consists of a grid of juxtaposed Tesseroid units in spherical coordinates with constant top and bottom surfaces. $\Delta\lambda$, $\Delta\varphi$ are mesh intervals in longitude and latitude directions, Δr is the thickness of the layer, $P_{(m,n)}$ is a computation point of observation surface in spherical coordinates, ρ_{ij} is the density of the Tesseroid numbered (i, j) in longitude and latitude directions.

Here, W is a positive scalar, which can be called distance-size radio [9]. The workflow to calculate gravitational acceleration of the computation point P by a Tesseroid is defined below:

Step01: Assume that W is given, the related parameters of d and L_{max} can be calculated by (9) and (14). Then, we can check that if (15) is available, the gravitational acceleration of point P generated by the Tesseroid can be calculated by (5) and (7) directly.

Step02: If (15) is unavailable, the Tesseroid should be subdivided into 8 new smaller Tesseroid units by the middle points of three different dimensions (Figure 2b).

Step03: As for the 8 new smaller Tesseroid units, repeat *step01* and *step02* until all Tesseroid units are available for (15) or sizes of the Tesseroid reach the given threshold. It is the recursive function of our algorithm, and the gravitational acceleration of the computation point by a Tesseroid is the accumulation of all the subdivided Tesseroid units.

B. GRAVITY MODELING OF A DENSITY LAYER IN SPHERICAL COORDINATES

Considering a 3D subsurface density layer, whose top and bottom surfaces are constant or variable in spherical coordinates, we divide the layer into a gird of M and N segments with equal mesh interval of $\Delta\lambda$, $\Delta\varphi$ in longitude and latitude directions. The total Tesseroid unit number of the layer is $N_{tess} = M \times N$.For the convenience of display, the top and bottom surfaces of the layer, and the observation surface are assummed to be constant in Figure 3.

The density of each Tesseroid is constant, which means only lateral difference of the spatial density distribution is available. The gravity anomaly of computation point P_{mn} can be described as a summation of each Tesseroid unit

$$g_{P_{mn}} = \sum_{j=1}^{N}\sum_{i=1}^{M} g(\rho_{(i,j)}), \quad i \in M, j \in N. \tag{16}$$

where, $g_{P_{mn}}$ is the gravity anomaly of the computation point P_{mn}, $g\left(\rho_{(i,j)}\right)$ is the forward gravity anomaly of the Tesseroid numbered (i, j) in longitude and latitude directions.

C. APPARENT DENSITY MAPPING IN SPHERICAL COORDINATES

Cordell and Henderson propose a space-domain, iterative approach to calculate the depth of the subsurface layer interface effectively [28]. We improved the algorithm for apparent density mapping. Assume that the subsurface layer is divided into M, N segments along the longitude, latitude directions with an equal mesh interval of $\Delta\lambda$, $\Delta\varphi$. $\phi_{k,(i,j)}$ is the density of the Tesseroid numbered (i, j)in the longitude, latitude directions at the kth iteration. Obviously, $\phi_{k,(i,j)}$ is a matrix of $M \times N (i \in M, j \in N.)$. The theoretical algorithm to obtain the density of each Tesseroid can be described as

$$\lim_{k\to\infty} \phi_{k,(i,j)} = \phi_{(i,j)}, \quad i \in M,\ j \in N. \tag{17}$$

The procedure of the apparent density mapping to seek the density of each Tesseroid is the follow steps:

Step01: Assume that the top and bottom interfaces of the layer are known in spherical coordinates, the observed gravity anomaly at each point is being generated by an infinite slab, and the observed gravity anomaly is known as a matrix $g_{obs(q)}$ with total number q. The initial density of each Tesseroid can be calculated as

$$\phi_{0,(i,j)} = \omega g_{obs(q)}, \quad i \in M,\ j \in N. \tag{18}$$

where, $\omega = 1/\left(2\pi G \Delta h_{(i,j)}\right)$, G is the Newtonian gravitational constant, $\Delta h_{(i,j)}$ is the thickness of the Tesseroid numbered (i, j) in the longitude, latitude directions.

Step02: To estimate next modification of the density of each Tesseroid cell, the gravity anomaly matrix $\mathbf{g}_{cal,0,q}$ can be calculated from density matrix $\phi_{0,(i,j)}$ by (16). The deviation of gravity anomaly is $\delta g_1 = g_{obs(q)} - g_{cal,0,q}$, and the new modified density of each Tesseroid $\phi_{1,(i,j)}$ can be generated as:

$$\phi_{1,(i,j)} = \phi_{0,(i,j)} + \omega \delta g_1, \quad i \in M,\ j \in N. \tag{19}$$

Similarly, for kth iteration, the deviation of gravity anomaly is $\delta g_k = g_{obs(q)} - g_{cal,k-1,q}$, and the modified density of each Tesseroid cell $\phi_{k,(i,j)}$ can be defined as

$$\phi_{k,(i,j)} = \phi_{k-1,(i,j)} + \omega \delta g_k, \quad i \in M,\ j \in N. \tag{20}$$

Step03: Renew the gravity anomaly matrix $\mathbf{g}_{cal,k,q}$ at kth iteration of the density model matrix $\phi_{k,(i,j)}$ by (16), and then renew the deviation of gravity anomaly

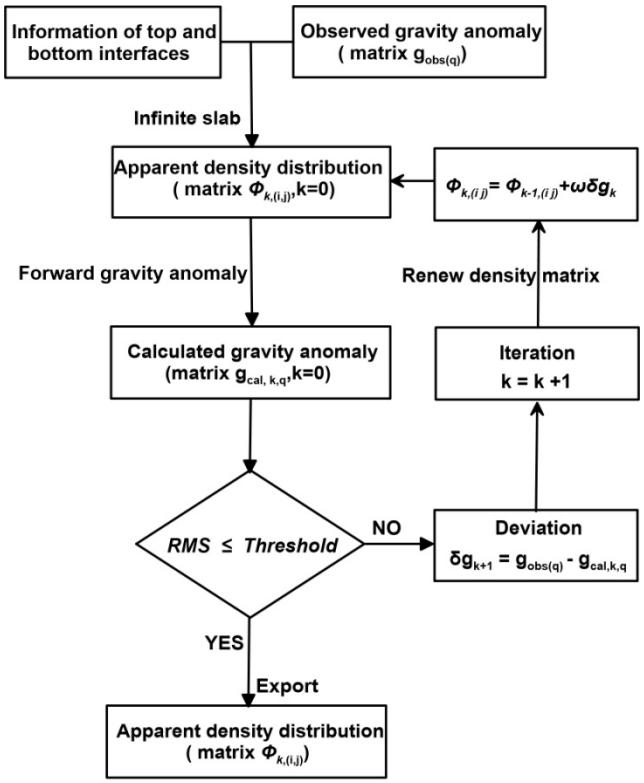

FIGURE 4. The flow diagram of the apparent density mapping in spherical coordinates.

$\delta g_{k+1} = g_{obs(q)} - g_{cal,k,q}$. We can obtain the density of each Tesseroid cell $\phi_{k+1,(i,j)}$ by (20).

Step04: Calculate the root mean square (RMS) between the observed gravity anomaly $g_{obs(q)}$ and the calculated gravity anomaly $g_{cal,k,q}$ for the kth iteration. This is

$$RMS = \sqrt{\sum_{i=1}^{q} \left(g_{obs(q)} - g_{cal,k}\right)^2 \Big/ q}. \tag{21}$$

The target of the iteration is to minimize RMS.

Step05: Repeat the steps above until RMS reach a specified tolerance or the iteration number reaches the given threshold. When the iteration stops, the $\phi_{k,(i,j)}$ is considered as the apparent density distribution of the subsurface layer in spherical coordinates. In terms of the density in our approach is the density contrast, the final apparent density can be obtained by adding a background density constant, such as 2.67g/cm^3.

III. THE SYNTHETIC DATA TESTS

A. PRECISION EVALUATION ON THE SPHERICAL SHELL

In general, the precision can be affected by many parameters, such as W, size of the Tesseroid, and Gauss-Legendre nodes. We create a homogenous spherical shell, which has analytical solutions to calculate the gravitational acceleration [29], [30] and can be perfectly subdivided into Tesseroids as well. The true gravitational acceleration of computation point P caused by the spherical shell can be written as:

$$g_p = \frac{4}{3}G\rho\frac{1}{R_p^2}\begin{cases} R_2^3 - R_1^3, & R_p \geq R_2 \\ 0, & R_p \leq R_1. \end{cases} \tag{22}$$

where, G is the Newtonian gravitational constant, and R_p is the geocentric distance from the center of the sphere to the computation point P. Assume that the thickness of the spherical shell is 30km with the radii of the outer and inner surfaces (R_2 = 6371km R_1 = 6341km), and the constant density of the spherical shell is ρ = 2.67 g/cm^3. The precision is very high when R_p is much bigger then R_2 [9]. In this paper, we pay more attention to the precision of the computation point P when it is located in the near surface of the spherical shell. The computation point P is supposed at the top of the spherical shell ($R_2 = R_p$) with longitude and latitude (120°E, 45° N), the precision caused by different values of the R_p and latitude will be discussed later. Then, the true gravitational acceleration of the computation point P generated by the spherical shell is 6682.232575mGal based on (22).

Figure 5 shows the errors between the shell effect and computed Tesseroid of the values of the distance size radio (W) varying from 1 to 2 with 0.1 intervals. We choose the W is bigger than 1 to make sure that the distance between point masses is not greater than the distance to the computation point [21]. Furthermore, the shell can be divided into different sizes of the Tesseroids, such as 2° × 2°, 1° × 1°, 30′ × 30′, 15′ × 15′. (a),(b),(c),(d) are the results with(a): $I = 3, J = 3$ (b): $I = 4, J = 4$ (c): $I = 5, J = 5$ (d): $I = 6, J = 6$. I and J are the Gauss-Legendre nodes in longitude and latitude directions, respectively. In general, the precision will be improved with bigger Gauss-Legendre nodes and smaller size of divided Tesseroids when the computation point P at the top of the shell.

Subsequently, we test the absolute errors between the shell effect and computed Tesseroid of different values of the R_p and latitude with constant Tesseroid grid size 1° × 1° and constant W = 1.5. Figure 6a shows the errors of different values of R_p. Height in lateral axis means the distance of the computation point P above the shell (Height = R_p-R_2). The range of the Height varies from 0 to 2km with 0.1km intervals. Specifically, when the computation point p is at the top of the shell (Height = 0), it is a singular problem and has been mentioned by scholars [31]–[35]. The precision of our algorithm has been improved vastly when the computation point P in the near surface of the shell (Figure 6a). Figure 6b shows the errors of different values of latitude varying from −90 to 90 with 10 intervals of the Height = 0. The precision is symmetrical with respect to equator. Although the errors have some shake along the latitude, the precision can be improved with more Gauss-Legendre nodes.

The precision of our approach to calculate the gravitational acceleration generated by Tesseroid is better than *Uieda at al.* [9], especially when the computation point P in the near surface of the model. Theoretically, the maximum absolute error can be controlled within 0.063mGal when

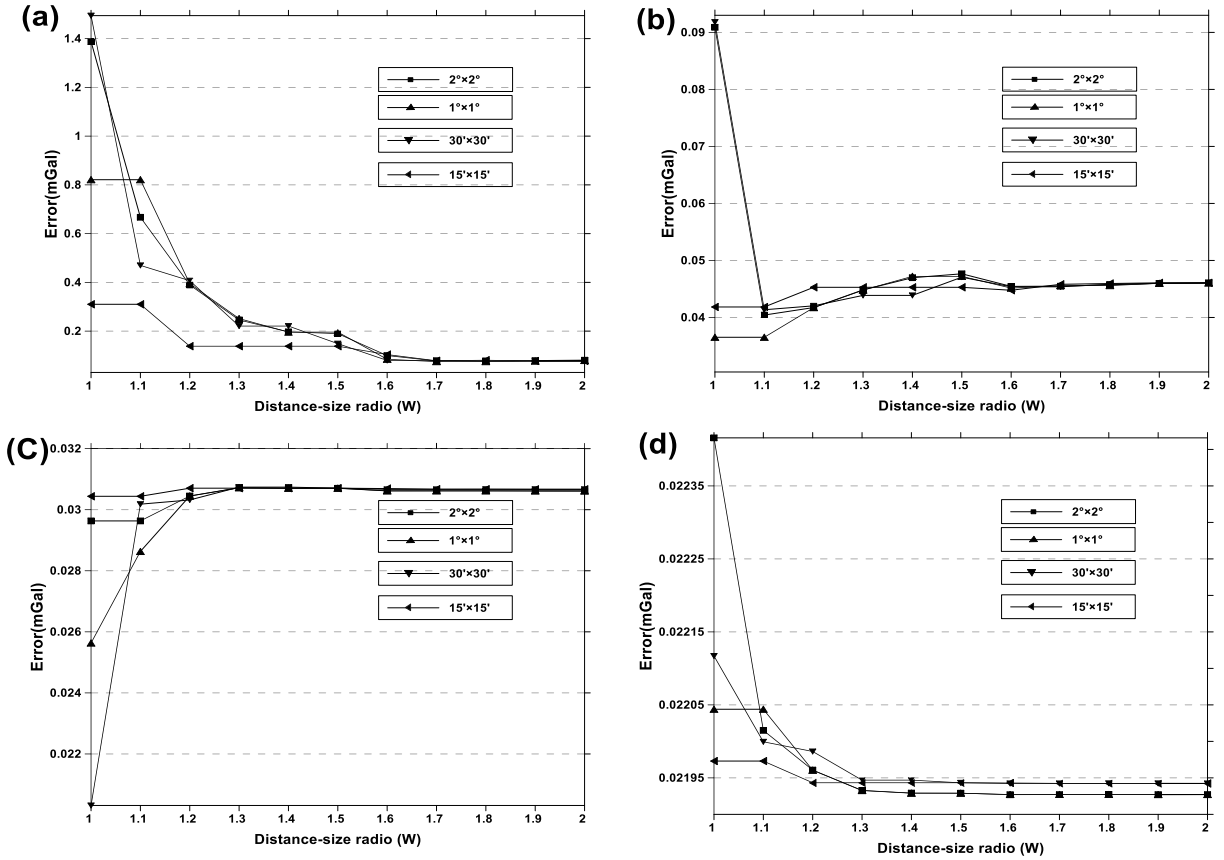

FIGURE 5. show the errors between the shell effect and computed Tesseroid of the values of the distance size radio (W) varying from 1 to 2 with 0.1 intervals. We choose the W is bigger than 1 to make sure that the distance between point masses is not greater than the distance to the computer point. Furthermore, the shell can be divided into different sizes of the Tesseroids, such as 2° × 2°, 1° × 1°, 30′ × 30′, 15′ × 15′. (a),(b),(c),(d) are the results of different Gauss-Legendre nodes $I \times J$,respectively, with(a): $I = 3, J = 3$ (b): $I = 4, J = 4$ (c): $I = 5, J = 5$ (d): $I = 6, J = 6$. I and J are the Gauss-Legendre nodes in longitude and latitude directions, respectively. In general, the precision will be improved with bigger Gauss-Legendre nodes and smaller size of divided Tesseroids when the computation point P at the top of the shell.

Height = 0 if the Gauss-Legendre nodes is bigger or equal to (4, 4) in the longitude and latitude directions, respectively, and the Tesseroid grid mesh is less than or equal to 1° × 1°. In this paper, The Gauss-Legendre nodes will be set as (4, 4) in the longitude and latitude directions and the parameter W will be set as 1.5 for subsequent calculation, the relative error can be controlled in 0.000943% =0.063/6628.232575.

B. DATA TEST ON A SYNTHETIC DENSITY LAYER

In this paper, we propose a synthetic model similar to Guo *et al.* [6]. Unlike the model presented by [6] in Cartesian coordinates, our synthetic density layer is simulated in spherical coordinates with undulant top and bottom interfaces. The range of the synthetic model is 100° -110°E, 25° -35° N, which has a grid of 41×41 with a equal interval of 0.25° in the longitude and latitude directions. The lateral residual density distribution of the layer, the range of which varies from $-0.1841 g/cm^3$ to $0.1462 g/cm^3$, is low in the west and high in the east (Figure 7a). The range of the top interface varies from 50m to 2070m (Figure 7b), and the lateral distribution of the bottom interface can be regard as the Moho surface with the range varying from 29380m to 43530m (Figure 7c). The theoretical gravity anomaly of the subsurface density layer on the constant observational arc-surface with an elevation 0m can be calculated by (18). The range of the theoretical gravity anomaly is from −246.0mGal to 163.8mGal with low in the west and high in the east (Figure 7d).

Subsequently, the theoretical gravity anomaly can be considered as observed gravity anomaly, and we implement the algorithm presented in this paper for apparent density mapping on the density layer. Figure 8a shows a well convergence curve of the mapping approach between the RMS and iteration number. Figure 8b shows the density distribution of the presented approach after 10 iterations, which is very close to the true model (Figure 7a). The deviation between the mapped density distribution and the true model is extremely small, which can be shown in Figure 8c with a maximum deviation $0.0019 g/cm^3$. Furthermore, the calculated gravity anomaly after 10 iterations (Figure 8d) is very close to the observed gravity anomaly (Figure 7d). The maximum deviation between the calculated gravity anomaly and the observed gravity anomaly is 0.144mGal (Figure 8e). The results of

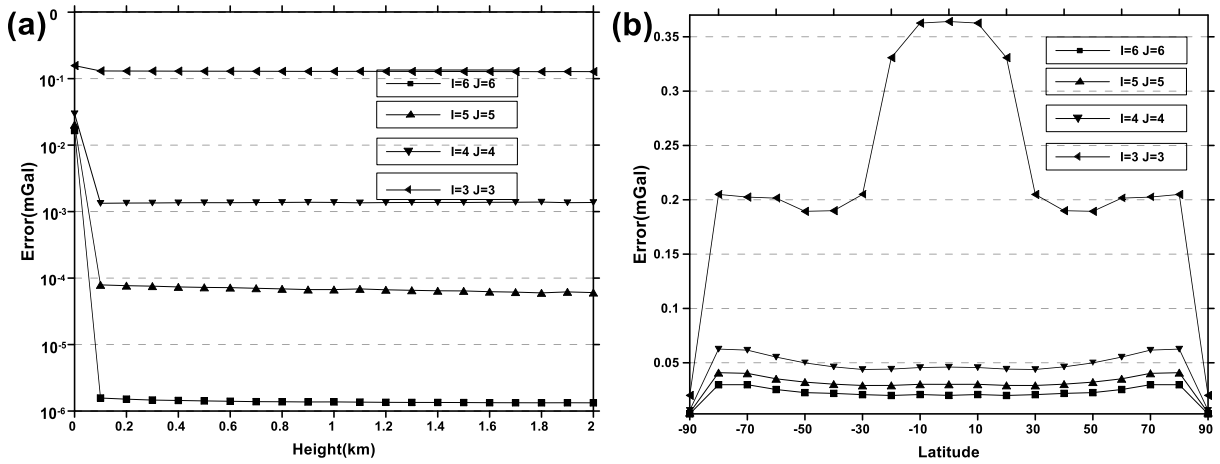

FIGURE 6. The absolute errors between the computed Tesseroid and shell effect with constant Tesseroid gird size 1° × 1° and constant W = 1.5. I and J are the Gauss-Legendre nodes in longitude and latitude directions, respectively. (a) The errors of different values of Rp (Height = Rp-R_2), the values of Height varying from 0 to 2km with 0.1km intervals. (b) The errors of different values of latitude varying from −90 to 90 with 10 intervals of Height = 0.

the apparent density mapping by our approach show a high precision and verify the feasibility directly.

We also compare our method with the traditional method in Cartesian coordinates, which divides the subsurface layer into vertical juxtaposed prisms. The results of traditional method can be seen in new Figure 8f and Figure 8g. Figure 8f is the results of the density distribution by traditional approach after 10 iterations and the maximum deviation from the true model reaches 0.0102 g/cm^3 in Figure 8g. In addition, we extract a profile AA′ to compare the results of different methods in Figure 8h. Compared to the traditional method without considering the curvature of the earth, the density distribution by our approach is closer to the true model.

IV. APPLICATION IN CHINESE MAINLAND

A. DATA SOURCES

Chinese mainland, which located on the collision zones between Indian and Eurasian Plates with an estimated area of 9.6 million km^2, is a westward subduction of Pacific Plate. The approximate range of Chinese mainland is 73° -136°E and 18° -54° N in geography. The units of China have diverse origins and complex histories of amalgamation and much attention has been received for last decades. For that continental scale, the curvature of the earth can not be ignored if we want to obtain more precious results. Hence, we used apparent density mapping approach in spherical coordinates presented in this paper for crustal apparent density mapping of Chinese mainland.

First, the Bouguer gravity anomalies of Chinese mainland and the adjacent areas can be obtained from the database of the world gravity map WGM2012 [36]. We assembled the Bouguer data area span 70° - 140°E and 15° - 58° N, which has a grid of 281 × 173 with equal interval 0.25° in longitude and latitude directions. The high frequency noise of the Bouguer gravity anomaly is mainly generated by shallow geological units and terrain correction. Thus, a low-pass filter of 200km wavelength is used to suppress the high frequency noise, and the final Bouguer gravity anomaly of Chinese mainland and the adjacent areas is in Figure 9a.

Secondly, the undulating terrain in the study area can be regarded as the upper interface of the layer, which can be assembled from ETOPO1 model [37]. The smooth filter is used to suppress the high frequency and the final upper interface of the study area is in Figure 9b.Meanwhile, we assume the upper interface is the observation surface in spherical coordinates. In addition, the quality of the Moho interface with the study area plays an important role on the results of crustal apparent density mapping. Models of the crustal thickness or Moho depth in Chinese mainland have been derived by different geophysical methods in recent years, such as seismic refraction/reflection, gravity field, surface wave, and body wave tomography studies [38]–[43]. Although the details of the crustal thickness or Moho depth are different, the general agreements have been reached among these studies. In this paper, we choose the Moho model obtained by *He R. et al.* from receiver function analysis, and the distribution of the seismic stations can be seen in Figure 9c [43]. The seismic stations are well in the east of China, whereas fewer stations coverage in the west, such as Tibetan Plateau. What is worse, there are no seismic stations in the adjacent areas of Chinese mainland. To obtain more precision Moho model of Chinese mainland and adjacent areas for our study area, another Moho model called CRUST1.0 with a resolution of 1° [44] in a global map is used to increase the precision and quality of our Moho model, especially in the west China and the adjacent areas of the Chinese mainland. The Moho depth of CRUST1.0 with respect to sea level is based on a new database from active source seismic studies and receiver function studies. The Moho depth, which combines the models of *He R. et al.* and CRUST1.0 in our study area, can be seen in Figure 9d.

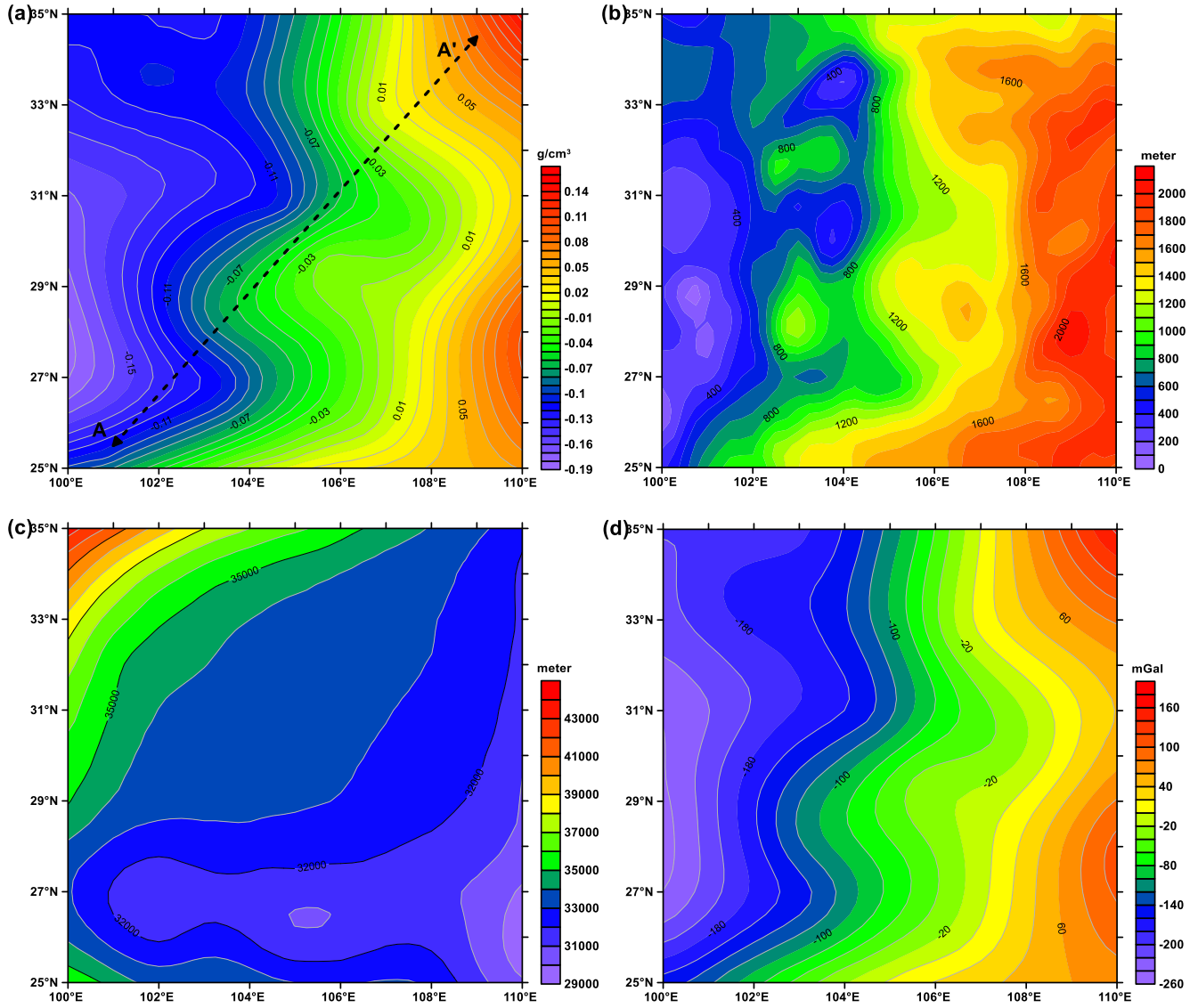

FIGURE 7. The synthetic model and its gravity anomaly in spherical coordinates, (a) the lateral residual density distribution, (b) the depth of the top interface, (c) the depth of the bottom interface, (d) the gravity anomaly on the constant observational arc-surface with an elevation of 0m.

B. CRUSTAL APPARENT DENSITY MAPPING

The calculated gravity anomaly, the deviation between the Bouguer gravity anomaly and calculated gravity anomaly, and the crustal apparent density distribution of Chinese mainland after 10 iterations with RMS = 0.284mGal can be seen in Figure 10a, Figure 10b and Figure 10c, respectively. The calculated gravity anomaly (Figure 10a) is similar to the Bouguer gravity anomaly (Figure. 9a) in Chinese mainland. The deviation from the gravity anomalies between the Bouguer gravity anomaly and calculated gravity anomaly (Figure 10b) varying from −0.5mGal to 0.5mGal, which show a good fitting for the Bouguer gravity anomaly in Chinese mainland. The range of the crustal apparent density of Chinese mainland varying from 2.45g/cm^3 to 2.81 g/cm^3 with respect to a background density 2.67 g/cm^3 (Figure 10c).

C. INTERPRETATON AND DISCUSSION

We combine the crustal apparent density distribution of the Chinese mainland with the regional lithologic units and geological boundaries of Chinese mainland, which is displayed in Figure 10c. The crustal apparent density mapping of Chinese mainland is generally low in the west and high in the east. It can be roughly divided into three regions from west to east, including western region, central region and eastern region.

1) WESTERN REGION

The western region mainly consists of Tibetan Plateau in the southwest Chinese mainland and Xinjiang Plate in the northwest Chinese mainland. The crustal apparent density distribution of the western region is generally in the low value area(less than 2.67 g/cm^3).

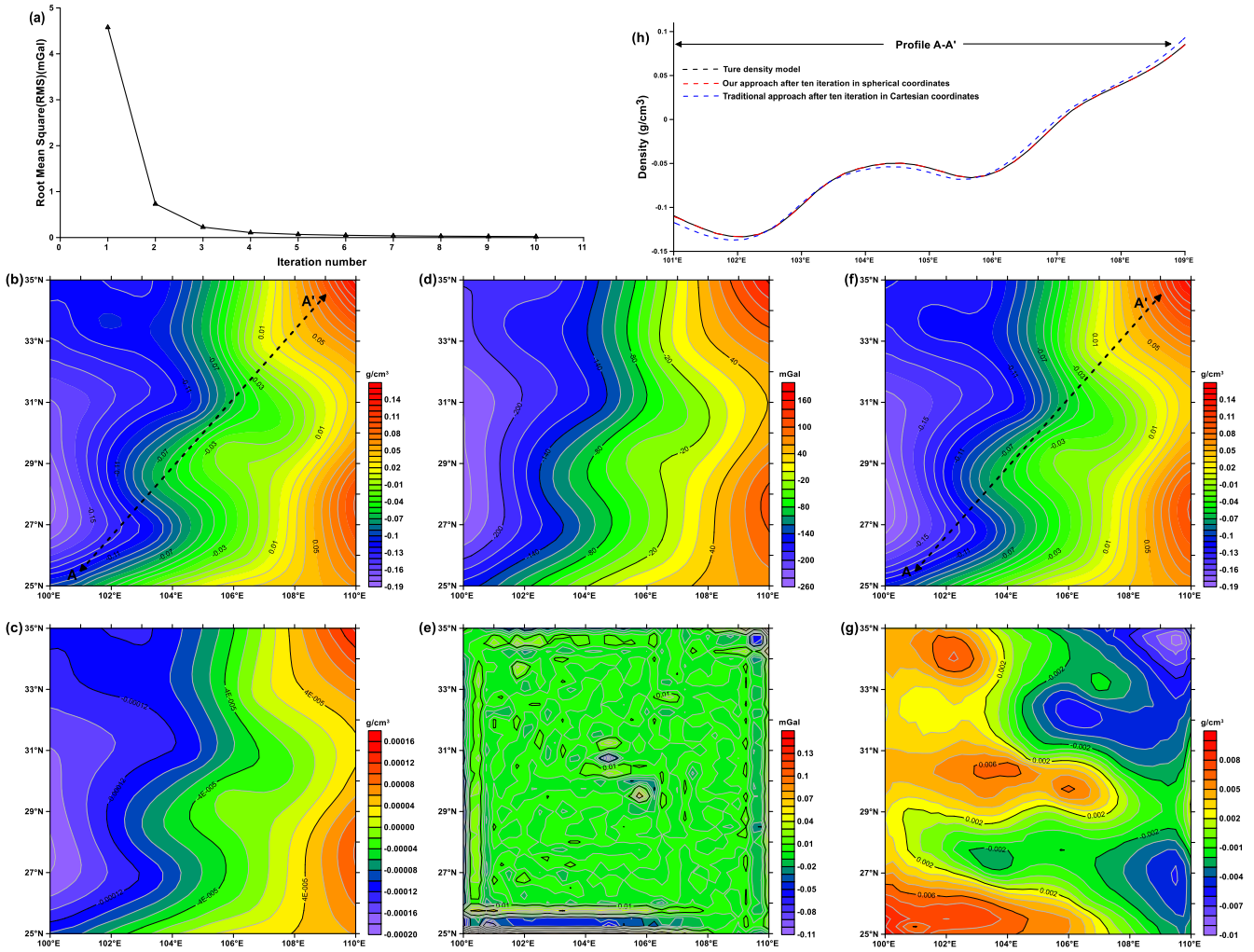

FIGURE 8. **(a) The convergence curve of the presented space-domain, iterative algorithm between the RMS and iteration number. (b), (c), (d), (e) are the results of the apparent density mapping by our approach after 10 iterations: (b) the mapped density distribution and (c)its deviation from the true density model(Fig.7a), (d) the calculated gravity anomaly of mapped density distribution and (e)its deviation from the observed gravity anomaly(Fig. 7d); (f), (g) are the results of the apparent density mapping by traditional method in Cartesian coordinates after 10 interations,(f) the mapped density distribution and (g)its deviation from the true density model(Fig.7a); (h) the density distribution of profile AA′, while the black dashed line is the true density model (Fig.7a), the red dashed line is the density model by our approach(Fig 8b) and the blue dashed line is the density model by traditional approach(Fig. 8f).**

Tibetan Plateau is in the front of the collision areas between the Indian plate and the Eurasian plate with a crustal thickness that reaches above 75km, mainly including HT, LT, QT and ST from south to north. The direction of mainly geological structures is EW. The crustal apparent density distribution of the Tibetan Plateau varies from 2.45-2.65 g/cm^3, and the average crustal apparent density is 2.51 g/cm^3. The crustal apparent density is the lowest with a value of 2.45 g/cm^3 in the transition area between the ST and West-Gunlun Organ, and then increases gradually to the central, eastern and southern areas of Tibetan Plateau. Due to the thinning of the Moho thickness in the east of HT, the maximum crustal apparent density of Tibetan Plateau can reach 2.65 g/cm^3. The results of the crustal apparent density distribution show a good response to the boundary position of terranes in this area.

Xinjiang Plate is comprised of the Tarim Basin, Tienshan Organ, Turpan Basin(TB) and Jungger Basin (JGB) from south to north, and the main directions of the Xinjiang Plate are EW and NNW. The crustal apparent density ranges from 2.58 g/cm^3 to 2.68 g/cm^3. Due to the equilibrium theory, the crustal thickness is thinned in the basin areas, such as Tarim Basin and JGB (Figure. 9d). Hence, the value of the crustal apparent density is obviously higher than that of adjacent areas. The maximum crustal apparent density can reach 2.68 g/cm^3 in JGB. Meanwhile, the boundary of basins can be clearly delineated by the value of the crustal apparent density distribution.

2) CENTRAL REGION

The central region is a transitional region between east region and west region with the value of crustal apparent density

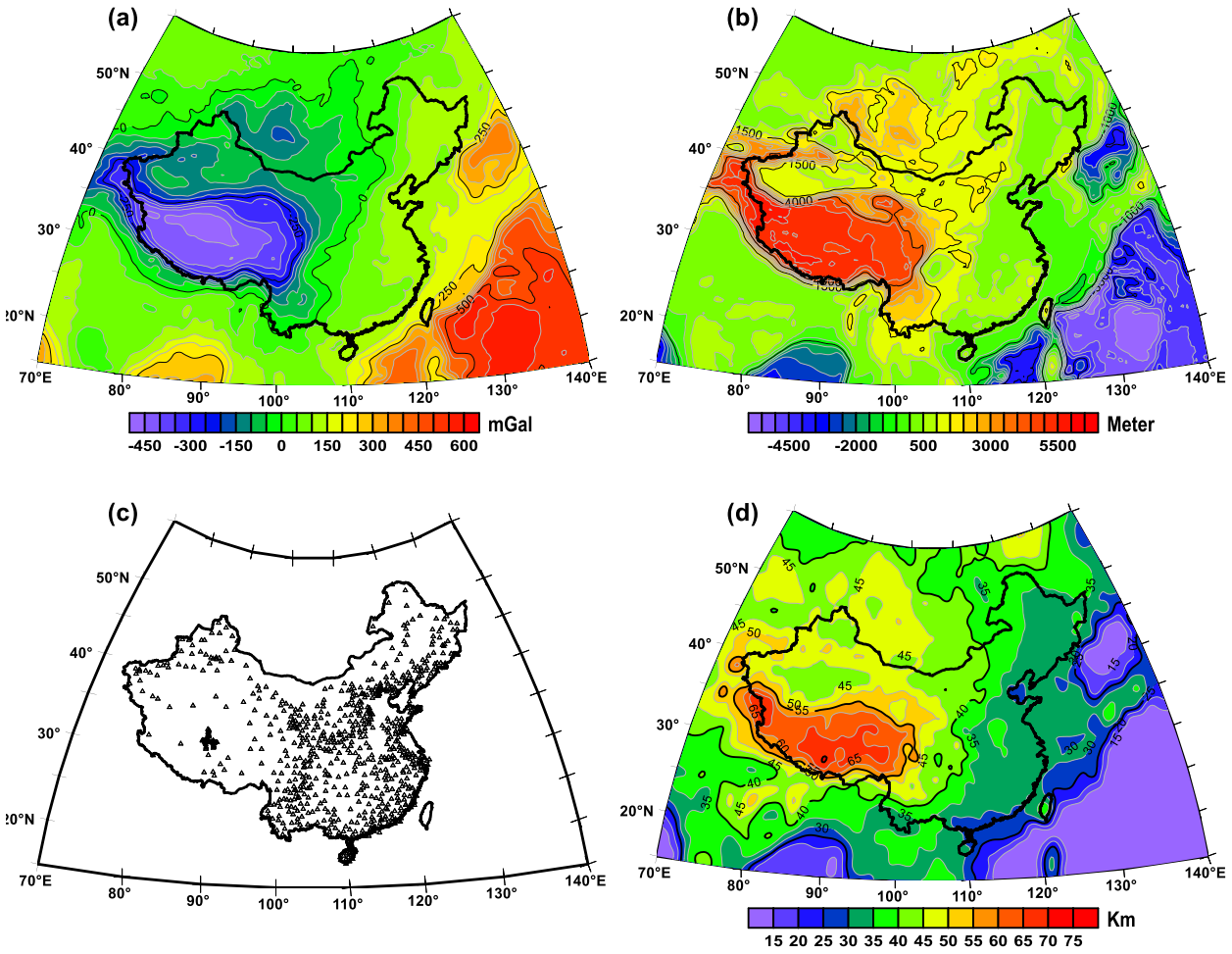

FIGURE 9. The black solid line is the boundary of Chinese mainland: (a) The Bouguer gravity anomaly of Chinese mainland and the adjacent areas. (b) The upper interface of Chinese mainland and the adjacent areas. (c) The distribution of the seismic stations in Chinese mainland by He R et al.. (d) The Moho depth of Chinese mainland and the adjacent areas which combines the models of He R. et al. and CRUST1.0.

varying from 2.52 g/cm^3 to 2.75 g/cm^3, mainly including Qaidam Basin (QB), Kunlun–Qaidam Terrane (KT), Qulianshan Orogon, East-Gunlun Orogon and Qinling -Dabie Orogon. The Qulianshan Orogon is the boundary of the North China Carton (NCC) and KT in the northwest of the central region, and East-Gunlun Orogon is the boundary of ST and KT in the southwest of the central region. Qinlin-DabieOrogon, located in the east of the central region, is the boundary which separated the South China Block (SCB) and NCC. The crustal apparent density is low in the west and high in the east, and the result of the crustal apparent density distribution effectively reflects the near EW tectonic strikes and the boundaries of the plates.

3) EASTERN REGION

The eastern region, which mainly in east of Chinese mainland, is mainly consist of SCB, NCC, SLB and Daxing'anling from the south to north. Due to the westward subduction of Pacific Plate in Chinese mainland, the crustal thickness decrease gradually from the western inland to the eastern coastline. The average value of the crustal apparent density is higher than 2.67g/cm^3.

The SCB is located in the southeastern part of Chinese mainland, mainly including Yangtaze Craton in the northwest and Cathaysia Block in the southeast. It is separated by the Qinlin-Dabie Orogon in the north, the Longmenshan Fault in the west, the Pacific plate in the southeast, and the South China Sea in the south, respectively. The crustal apparent density of SCB increases from northwest to southeast varying from 2.58-2.81 g/cm^3. Sichuan Basin(SB), located in the northwest of SCB, can be clearly delineated in Figure 9c from the value of the crustal density apparent. Furthermore, Jiao-Shao Fault, located in the east of SCB, which is the northeast boundary between Yangtze Craton and Cathaysia Block, and Cathaysia Fold belt, located in the center of Cathaysia Block can delineated in Figure 10c.

The NCC, as one of the oldest carton in the world, is separated by Qulianshan Orogon in the west, Qinling-Dabie Orogon in the north, the Pacific plate in the east, and Yinshan-Yanshan Orogon in the north, respectively. The NCC consists

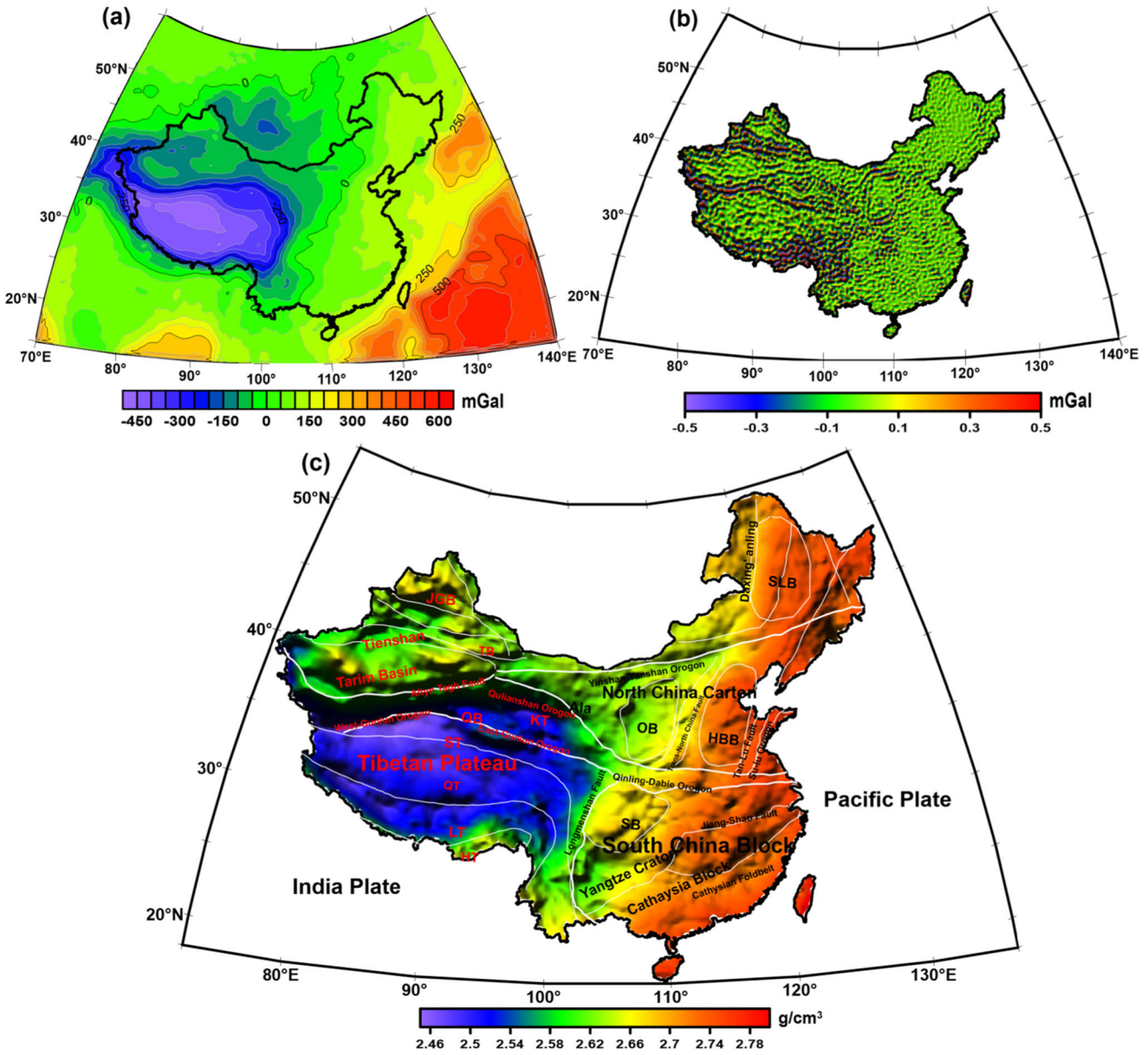

FIGURE 10. The results of Chinese mainland after 10 iterations with RMS = 0.284mGal. (a) the calculated gravity anomaly of Chinese mainland.(b) the deviation from the gravity anomalies between the Bouguer gravity anomaly and calculated gravity anomaly.(c) the crustal apparent density distribution and the lithologic units and geological boundaries of Chinese mainland. The white lines are the geological tectonic lines or plate boundaries. HT:Himalayan Terrane; LT:LhasaTerrane; QT:Qiangtang Terrane; ST:Songpan–Ganzi Terrane; TB: Turpan Basin; JGB: Jungger Basin; QB:Qaidam Basin; KT: Kunlun–Qaidam Terrane ;SB:Sichuan Basin; Ala: Alashan Block; OB: Ordos Block; HBB: Huabei Block; SLB:Songliao Basin.

of three major parts: the western NCC, Trans-North China Fault (the central NCC) and the eastern NCC [45] The western NCC, mainly including Alashan Block (Ala) and Ordos Block (OB), shows a low crustal apparent density. The average crustal apparent density is 2.63 g/cm^3. Whereas, the eastern NCC, which is mainly consists of Huabei Block(HBB), Tanlu Fault and Sulu Orogon shows a high crustal apparent density.

The SLB and Daxing'anling are located in the northeast of Chinese mainland. In the western part of Daxing'anling, the tectonic evolution is dominated by the Mongolia-Okhotsk tectonic belt, supplemented by the Pacific tectonic domain, and the average crustal apparent density is 2.68g/cm^3. The eastern side of Daxing'anling is mainly affected by the subduction of the Pacific Plate. The crustal apparent density increases from inland to coastal areas, and the average crustal apparent density of SLB reaches 2.73g/cm^3.

V. CONCLUSION

We have presented a modified algorithm (2-GLQ) to forward the gravity anomaly generated by an arbitrary Tesseroid in spherical coordinates. The numerical results can be

controlled by lesser weighted points, and both the precision and computation time have been improved vastly. In addition, we have implemented a modified adaptive recursive algorithm to improve the precision when the computation points in the near surface of the Tesseroid.

In order to verify the precision of the present method, a homogenous spherical shell was created to compare the errors between the shell effect and computed Tesseroid. We have tested the correlations between parameter W, number of the Gauss-Legendre nodes and the sizes of Tesseroids. In general, the precision can be improved with more Gauss-Legendre nodes and smaller size of Tesseroids. The relative error can be controlled in 0.0009343% when the Gauss-Legendre nodes are set as (4, 4) in the longitude and latitude directions and the parameter W is set as 1.5. The precision has been improved greatly compared to previous results [9].

We have presented an apparent density mapping approach based on a subsurface density layer in spherical coordinates. The synthetic data tests show that our approach is easy to convergence and has high precision. Compared to the traditional method without considering the curvature of the earth, the density distribution by our approach is closer to the true model. The synthetic data tests verified the feasibility of the presented approach.

In real application, Chinese mainland is a vast continent with spans more than 60° and 30° in longitude and latitude directions, respectively. Thus, the apparent density mapping with considering the curvature of the earth is closer to the actual results. The crustal apparent density of Chinese mainland is low in the west and high in the east varying from 2.45g/cm^3 to 2.81 g/cm^3. Alternatively, the results of crustal apparent density mapping correspond well with regional lithologic units and geological boundaries, and can also provide assistance for further study of regional tectonics and geological structures.

ACKNOWLEDGMENT

The authors would like to thank *He R. et al.* for providing the Moho data of Chinese mainland. The authors would like to thank the editor Jenny Mahoney and three anonymous reviewers for their constructive suggestions to improve the manuscript.

REFERENCES

[1] H. Granser, "Deconvolution of gravity data due to lateral density distributions," *Geoexploration*, vol. 23, no. 4, pp. 537–547, Dec. 1985, doi: 10.1016/0016-7142(85)90080-8.

[2] H. Granser, B. Meurers, and P. Steinhauser, "Apparent density mapping and 3D gravity inversion in the Eastern Alps," *Geophys. Prospecting*, vol. 37, no. 3, pp. 279–292, Apr. 1989, doi: 10.1111/j.1365-2478.1989.tb02207.x.

[3] P. Keating, "Density mapping from gravity data using the Walsh transform," *Geophysics.*, vol. 57, no. 4, pp. 637–642, Apr. 1992, doi: 10.1190/1.1443276.

[4] D.-S. Xu, H.-L. Zeng, and T.-F. Wan, "Apparent density mapping and tectonic of China," (in Chinese), *Earth Sci. Frontiers*, vol. 8, no. 2, pp. 407–414, 2001.

[5] J. B. C. Silva, F. S. Oliveira, V. C. F. Barbosa, and H. F. C. Velho, "Apparent-density mapping using entropic regularization," *Geophysics*, vol. 72, no. 4, pp. 151–160, Jul. 2007, doi: 10.1190/1.2732557.

[6] L. Guo, L. Shi, and S. Li, "A wavenumber-domain iterative approach for apparent density mapping of an undulant layer and its application in central South China," *Geophysics*, vol. 84, no. 1, pp. 1–38, Oct. 2018. [Online]. Available: https://www.researchgate.net/publication/328079462

[7] L. Cordell and A. E. McCafferty, "A terracing operator for physical property mapping with potential field data," *Geophysics*, vol. 54, no. 5, pp. 621–634, May 1989, doi: 10.1190/1.1442689.

[8] T. Grombein, K. Seitz, and B. Heck, "Optimized formulas for the gravitational field of a tesseroid," *J. Geodesy*, vol. 87, no. 7, pp. 645–660, Jul. 2013, doi: 10.1007/s00190-013-0636-1.

[9] L. Uieda, V. C. F. Barbosa, and C. Braitenberg, "Tesseroids: Forward-modeling gravitational fields in spherical coordinates," *Geophysics*, vol. 81, no. 5, pp. 41–48, Sep. 2016, doi: 10.1190/geo2015-0204.1.

[10] E. G. Anderson, *The effect of Topography on Solutions of Stokes' Problem* (UNISURV Report). Kensington, NSW, Australia: School of Surveying, University of New South Wales, 1976.

[11] T. R. LaFehr, "An exact solution for the gravity curvature (Bullard B) correction," *Geophysics*, vol. 56, no. 8, pp. 1179–1184, Aug. 1991, doi: 10.1190/1.1443138.

[12] J. Mikuška, R. Pašteka, and I. Marušiak, "Estimation of distant relief effect in gravimetry," *Geophysics*, vol. 71, no. 6, pp. J59–J69, Nov. 2006, doi: 10.1190/1.2338333.

[13] D. Tsoulis, "Analytical and numerical methods in gravity field modelling of ideal and real masses," Ph.D. dissertation, Deutsche Geodätische Kommission, Munich, Germany, 1991.

[14] B. Heck and K. Seitz, "A comparison of the tesseroid, prism and point-mass approaches for mass reductions in gravity field modelling," *J. Geodesy*, vol. 81, no. 2, pp. 121–136, Feb. 2007, doi: 10.1007/s00190-006-0094-0.

[15] F. Wild-Pfeiffer, "A comparison of different mass elements for use in gravity gradiometry," *J. Geodesy*, vol. 82, no. 10, pp. 637–653, Oct. 2008, doi: 10.1007/s00190-008-0219-8.

[16] W.-B. Shen and X.-L. Deng, "Evaluation of the fourth-order tesseroid formula and new combination approach to precisely determine gravitational potential," *Studia Geophysica Et Geodaetica*, vol. 60, no. 4, pp. 583–607, Oct. 2016, doi: 10.1007/s11200-016-0402-y.

[17] C. Hirt and M. Kuhn, "Band-limited topographic mass distribution generates full-spectrum gravity field: Gravity forward modeling in the spectral and spatial domains revisited," *J. Geophys. Res.*, vol. 119, no. 4, pp. 3646–3661, Apr. 2014, doi: 10.1002/2013JB010900.

[18] Z. Li, T. Hao, Y. Xu, and Y. Xu, "An efficient and adaptive approach for modeling gravity effects in spherical coordinates," *J. Appl. Geophys.*, vol. 73, no. 3, pp. 221–231, Mar. 2011, doi: 10.1016/j.jappgeo.2011.01.004.

[19] M. F. Asgharzadeh *et al.*, "Spherical prism gravity effects by Gauss-Legendre quadrature integration," *Geophys. J. Int.*, vol. 173, no. 1, pp. 315–333. Apr. 2008, doi: 10.1111/j.1365-246X.2007.03692.x.

[20] C. Roussel, J. Verdun, J. Cali, and F. Masson, "Complete gravity field of an ellipsoidal prism by Gauss–Legendre quadrature," *Geophys. J. Int.*, vol. 203, no. 3, pp. 2220–2236, Dec. 2015, doi: 10.1093/gji/ggv438.

[21] C. C. Ku, "A direct computation of gravity and magnetic anomalies caused by 2- and 3-dimensional bodies of arbitrary shape and arbitrary magnetic polarization by equivalent-point method and a simplified cubic spline," *Geophysics*, vol. 42, no. 3, pp. 610–622, Apr. 1997, doi: 10.1190/1.1440732.

[22] Q. Liang, C. Chen, and Y. Li, "3-D inversion of gravity data in spherical coordinates with application to the GRAIL data," *J. Geophys. Res. Planets*, vol. 119, no. 6, pp. 1359–1373, May 2014, doi: 10.1002/2014JE004626.

[23] Y. Zhang, Y. Wu, Y. Yan, H. Wang, J. Alexis, P. Rodriguez, and Y. Qiu, "3D inversion of full gravity gradient tensor data in spherical coordinate system using local north-oriented frame," *Earth, Planets Space*, vol. 70, p. 58, Apr. 2018, doi: 10.1186/s40623-018-0825-5.

[24] G. Zhao, B. Chen, L. Uieda, J. Liu, M. K. Kaban, L. Chen, and R. Guo, "Efficient 3-D large-scale forward modeling and inversion of gravitational fields in spherical coordinates with application to Lunar Mascons," *JGR Solid Earth*, vol. 124, no. 4, pp. 4157–4173, Apr. 2019, doi: 10.1029/2019JB017691.

[25] Z. Martinec, *Boundary-Value Problems for Gravimetric Determination of a Precise Geoid* (Lecture Notes in Earth Sciences), vol. 73. New York, NY, USA: Springer, 1998.

[26] A. H. Stroud and D. Secrest, *Gaussian Quadrature Formulas*. Upper Saddle River, NJ, USA: Prentice-Hall, 1966.

[27] R. R. B. von Frese, W. J. Hinze, L. W. Braile, and A. J. Luca, "Spherical-earth gravity and magnetic anomaly modeling by Gauss-Legendre quadrature integration," *J. Geophys.*, vol. 49, no. 3, p. 234-242, Feb. 1981.
[28] L. Cordell and R. G. Henderson, "Iterative three-dimensional solution of gravity anomaly data using a digital computer," *Geophysics*, vol. 33, no. 4, pp. 596–601, Aug. 1968, doi: 10.1190/1.1439955.
[29] P. Vaníček, P. Novák, and Z. Martinec, "Geoid, topography, and the Bouguer plate or shell," *J. Geodesy*, vol. 75, no. 4, pp. 210–215, Jul. 2001, doi: 10.1007/s001900100165.
[30] R. Karcol, "Gravitational attraction and potential of spherical shell with radially dependent density," *Studia Geophysica Et Geodaetica*, vol. 55, no. 1, pp. 21–34, Jan. 2011, doi: 10.1007/s11200-011-0002-9.
[31] R. Klees, "Numerical calculation of weakly singular surface integrals," *J. Geodesy*, vol. 70, no. 11, pp. 781–797, Nov. 1996, doi: 10.1007/BF00867156.
[32] R. Klees and R. Lehmann, "Calculation of strongly singular and hypersingular surface integrals," *J. Geodesy*, vol. 72, no. 9, pp. 530–546, Sep. 1998, doi: 10.1007/s001900050192.
[33] L. J. Gray, J. M. Glaeser, and T. Kaplan, "Direct evaluation of hypersingular Galerkin surface integrals," *SIAM J. Sci. Comput.*, vol. 25, no. 5, pp. 1534–1556, Jul. 2004, doi: 10.1137/S1064827502405999.
[34] M. A. Khayat and D. R. Wilton, "Numerical evaluation of singular and near-singular potential integrals," *IEEE Trans. Antennas Propag.*, vol. 53, no. 10, pp. 3180–3190, Oct. 2005, doi: 10.1109/TAP.2005.856342.
[35] M. G. D'Urso, "On the evaluation of the gravity effects of polyhedral bodies and a consistent treatment of related singularities," *J. Geodesy*, vol. 87, no. 3, pp. 239–252, Mar. 2013, doi: 10.1007/s00190-012-0592-1.
[36] G. Balmino, N. Vales, S. Bonvalot, and A. Briais, "Spherical harmonic modelling to ultra-high degree of Bouguer and isostatic anomalies," *J. Geodesy*, vol. 86, no. 7, pp. 499–520, Jul. 2012, doi: 10.1007/s00190-011-0533-4.
[37] C. Amante and B. W. Eakins, "ETOPO1 1 arc-minute global relief model," Procedures, Data Sources Anal., NOAA Tech. Memorandum NESDIS, Nat. Geophys. Data Center, NOAA, Silver Spring, MD, USA, Tech. Rep. NGDC-24, 2009.
[38] L. Bai, X. Tian, and J. Ritsema, "Crustal structure beneath the Indochina peninsula from teleseismic receiver functions," *Geophys. Res. Lett.*, vol. 37, no. 24, Dec. 2010, Art. no. L24308, doi: 10.1029/2010GL044874.
[39] L. H. Guo, X. H. Meng, L. Shi, and Z. Chen, "Preferential filtering method and its application to Bouguer gravity anomaly of Chinese continent," *Chin. J. Geophys.*, vol. 55, no. 12, pp. 4078–4088, Apr. 2012, doi: 10.6038/j.issn.0001-5733.2012.12.020.
[40] W. Stolk, M. Kaban, F. Beekman, M. Tesauro, W. D. Mooney, and S. Cloetingh, "High resolution regional crustal models from irregularly distributed data: Application to Asia and adjacent areas," *Tectonophysics*, vol. 602, no. 16, pp. 55–68, Aug. 2013, doi: 10.1016/j.tecto.2013.01.022.
[41] Y. Sun, M. N. Toksöz, S. Pei, and F. D. Morgan, "The layered shear-wave velocity structure of the crust and uppermost mantle in China," *Bull. Seismolog. Soc. Amer.*, vol. 98, no. 2, pp. 746–755, Apr. 2008, doi: 10.1785/0120050222.
[42] Y. Li, M. Gao, and Q. Wu, "Crustal thickness map of the Chinese mainland from teleseismic receiver functions," *Tectonophysics*, vol. 611, no. 25, pp. 51–60, Jan. 2014, doi: 10.1016/j.tecto.2013.11.019.
[43] R. He, X. Shang, C. Yu, H. Zhang, and R. D. Van der Hilst, "A unified map of Moho depth and V_p/V_s ratio of continental China by receiver function analysis," *Geophys. J. Int.*, vol. 199, no. 3, pp. 1910–1918, Dec. 2014, doi: 10.1093/gji/ggu365.
[44] G. Laske, G. Masters, Z. Ma, and M. Pasyanos, "Update on CRUST1.0—A 1-degree global model of earth's crust," *Geophys. Res. Abs.*, vol. 15, no. EGU2013-2658, Apr. 2013. [Online]. Available: http://igppweb.ucsd.edu/~gabi/crust1.html
[45] G. Zhao, S. A. Wilde, P. A. Cawood, and M. Sun, "Archean blocks and their boundaries in the North China Craton: Lithological, geochemical, structural and *P–T* path constraints and tectonic evolution," *Precambrian Res*, vol. 107, nos. 1–2, pp. 45–73, Mar. 2001, doi: 10.1016/S0301-9268(00)00154-6.

AOWEI HAO received the B.S. degree from the China University of Geosciences, Beijing, in 2015, where he is currently pursuing the M.S. degree in geophysics. He was an Assistant Engineer with the People's Armed Police Force, China, from 2015 to 2017. His research interests include gravity and magnetic data processing, and inversion algorithms. He is also interested in applications of machine learning in geophysics. In addition, he is planning to learn joint inversion of seismic and gravity data for further research.

LIANGHUI GUO was born in Fujian, China, in 1980. He received the B.S. and M.S. degrees in applied geophysics and the Ph.D. degree in applied geophysics from the China University of Geosciences, Beijing, China, in 2006 and 2012, respectively, where he is currently a Professor with the School of Geophysics and Information Technology. His research interests include fine processing and the inversion of gravity and magnetic data, joint inversion of seismic and gravity data, and their applications in the studies of deep structure and tectonics.

XIANG WANG received the B.S. and M.E. degrees from the China University of Geosciences, Beijing, in 2014 and 2019, respectively. He was an Assistant Engineer of Chinese People's Armed Police Force, from 2014 to 2016. He is currently an Assistant Engineer of China Geological Survey. His research interests include human–computer interaction, and gravity and magnetic inversion. In addition, he has a deep understanding of the joint inversion of seismic and gravity data.